Tip-Enhanced Infrared Imaging with Sub-10 nm Resolution and Hypersensitivity

Jian Li[1], Junghoon Jahng[2], Jie Pang[1], William Morrison[1], Jin Li[1], Eun Seong Lee[2], Jing-Juan Xu[1], Hong-Yuan Chen[1], Xing-Hua Xia[1]*.

1. State Key lab of Analytical Chemistry for Life Science, School of Chemistry and Chemical Engineering, Nanjing University, 210023 Nanjing, China
2. Center for nanocharacterization, Korea Research Institute of Standards and Science, Daejeon 34113, Republic of Korea
3. Molecular Vista Inc., 6840 Via Del Oro, Suite 110, San Jose, CA 95119, USA.

Corresponding author: X.H. Xia (xhxia@nju.edu.cn)

Contents

S1. Supplementary methods

S1.1 Reagents

SiO_2/Silicon wafer (SiO_2 thickness: 500 nm; resistance of Si: 1-15 Ω·cm) was bought from Suzhou Crystal Silicon Electronic & Tehchnology Co., Ltd. 16-Mercaptohexadecanoic acid (MDHA), 4-mercaptobenzoic acid(MBA) were purchased from Sigma-Aldrich. Bovine Serum Albumin (BSA) was purchased from Southern Biotechnology Associates, Inc., P. R. China. Other reagents and chemicals were of analytical grade. All reagents were used as received without further purification. MDHA and MBA solutions were prepared with ethanol and other solutions were prepared with Milli-Q water from a Millipore system.

S1.2 Instruments

AFM and PiFM were recorded on a VistaScope system (Molecular Vista, USA), and FTIR was collected on a Nicolet IS50 (Nicolet, USA). Vacuum evaporation of Au and Ag was carried out on a PVD75 Proline SP (Kurt, J Lesker, USA). Vacuum sputtering of Pt was carried out on a JEC-3000FC (JEOL, JP).

S1.3 Preparation of the metal films

Substrate was placed in a deposition cabin with the SiO_2 side facing the metal target. After tuning parameters, the desired thickness of metal film was achieved. After deposition, the metal film was washed with deionized water and dried by N_2.

S1.4 Preparation of the samples

For SAMs: Metal films were immersed in 10 mM MDHA and MBA solution respectively for 24 h. After modification, the SAMs were washed with ethanol and dried by N_2 sweeping. For the BSA layer, the gold film was dipped in 100 ng/mL BSA solution for 5 s and washed with deionized water following by drying with N_2 sweeping.

S1.5 Measurement of PiFM

PiFM measurements were taken on a VistaScope microscope that is coupled to a QCL laser system from Block Engineering with a wavenumber resolution of 1 cm^{-1} and a tuning range from 770 to 1885 cm^{-1}. The IR beam is focused on the sample with an angle of 30 degrees using a parabolic mirror, has a pulse duration of 40 ns and pulse energy of 0.1 μJ–2 μJ with incident wavelengths. The set point is set as 75% with an oscillation amplitude of ~1 nm. The microscope is operated in dynamic mode with NCH-Au 300 kHz non-contact cantilevers from Nanosensors. The cantilever was excited at its second resonance around 1.43 MHz. The measurements were carried out in an N_2 environment to minimize the water background from environment. The collection time for each spectrum is around 1s, and the time per image is about 2 min with 1 line/s speed at 128×128 resolution. The spectrum is normalized with the background laser power profile spectrum.

S1.6 IR characterization of molecules

ATR-FTIR spectra of each molecule were recorded on a Nicolet IS 50. IR detection was carried out with a homemade ATR accessory and the diameter of the detection cell was 6 mm. Unpolarized IR radiation was totally reflected at the ZnSe prism/solution interface with an incident angle θ=75° and was detected with a liquid-nitrogen-cooled MCT detector. After adding

the molecular solution into the accessory, the spectrum of each molecule was collected by taking the IR spectrum of ethanol (MDHA, MBA) or water (BSA) as the reference. For adsorption kinetics of BSA on Au film, a chemically prepared Au film was made on ZnSe prism as described in reference S1. The time-dependent ATR-surface enhanced infrared absorption spectra were recorded after the adding of 100 ng/mL BSA solution on prism surface by taking water spectrum as the reference. The spectral range was 4000-650 cm^{-1} with a resolution of 4 cm^{-1}.

S2. Simulations for the electromagnetic field distribution

According to the analytical theory of the field enhancement for the layered system **(***S2)*, the field enhancement at the tip end is rigorously calculated with respect to the SiO_2 substrate and a 90 nm Au film on SiO_2 as below. The simulation parameters are R = 15 nm, L = 300 nm, H = 1 nm, and the incident electric field E_0 is 3×10^5 V/m.

S3. Calculations for the tip-enhanced thermal expansion and the van der Waals force

Calculating the absorbed power inside the monolayer by $P_{abs} = \int a_{abs} \frac{1}{2} c\varepsilon_0 |E|^2 \, dV$ with the absorption coefficient of $a_{abs} = \frac{4\pi}{\lambda} \frac{9\mathrm{Re}[n]\mathrm{Im}[n]}{(\mathrm{Re}[n]^2 - \mathrm{Im}[n]^2)^2}$, one can estimate the thermal expansion of the monolayer. The σ_{ba}, ρ_{ba}, C_{ba}, and κ_{ba} are 173×10^{-6} K^{-1}, 1.5×10^{3} kg/m^3, 1202 J/kg·K and 0.151 W/m·K, respectively, for the benzoic acid. According to the reference *S3*, the maximum tip-enhanced thermal expansion can be estimated as:

$$\Delta L_{max} \approx \sigma d \Delta T_{max} \approx \frac{\sigma \tau_{rel}}{\rho C d} \int a_{abs} \frac{1}{2} c\varepsilon_0 |E|^2 \, dz. \quad \text{(S1)}$$

where σ is the linear thermal expansion coefficient and ΔT_{max} is given as $\Delta T_{max} \approx \frac{P_{abs}}{\rho C V_{heat}} \tau_{rel}$ for $\tau_{rel} < \tau_p$ and $\Delta T_{max} \approx \frac{P_{abs}}{\rho C V_{heat}} \tau_p$ for $\tau_{rel} > \tau_p$ *(S4)*. Because the thickness of the monolayer is around 1 nm, by integrating the electric field inside the monolayer, then one can obtain the ΔL of ~5 pm for the monolayer of benzoic acid at the vibrational resonance of 1694 cm^{-1}, where the refractive index is 1.45 and the extinction coefficient is 0.87 m^{-1}, resulted in the a_{abs} is 7.21 × 10^5 m^{-1}. The modulated van der Waals force due to thermal expansion are given as

$$\Delta F_{vDW} \approx -\frac{H_{eff} R}{6} \frac{1}{H^3} \Delta L \text{ (S2)}$$

where H_{eff}, R are the effective Hamaker constant and radius of the tip, respectively. The effective Hamaker constant between the Au tip and the benzoic acid is given as $H_{eff} = \sqrt{H_{Au} \times H_{ba}}$ = 14 × 10^{-20} J where H_{Au} is 45.3 × 10^{-20} J and H_{ba} is 4.3 × 10^{-20} J. Note that we implemented the Hamaker constant of the acetone or ethyl acetate as the H_{ba}, which has the similar van der Waals property *(S13)*. Then, the modulated van der Waals force due to the thermal expansion for ΔL = 5 pm is ~1.6 pN at H = 1 nm gap distance. On the other hand, on the SiO_2 substrate, the tip-enhanced thermal expansion of the MBA is reduced by ~ 0.2 pm which corresponds to ΔF_{vdW} ~ 0.07 pN at H = 1 nm gap distance.

The σ_{MDHA}, ρ_{MDHA}, C_{MDHA}, and κ_{MDHA} are 270×10^{-6} K^{-1}, 0.942×10^{3} kg/m^3, 1831.9 J/kg·K and 0.171 W/m·K, respectively, for the MDHA. The maximum tip-enhanced thermal expansion of MDHA whose thickness of the monolayer is around 2.5 nm can be estimated as 107 pm on Au film, which corresponds to the ΔF_{vdW} ~ 13 pN. However, ΔL of the MDHA is around 9 pm which corresponds to ΔF_{vdW} ~ 0.8 pN. Thus, the PiFM signals of the monolayers are barely measurable on SiO_2 substrate but they are well measurable on Au film, which corresponds to the experimental result.

All the parameters and where they are derived are listed in Table S1.

Table S1. Details of the parameters used for PiFM calculation

Parameters	Value	Adapted from	Value	Adapted from
	For MBA		For MDHA	
σ(Thermal expansion)	173×10^{-6} K^{-1}	Volume expansion coefficient of Benzoic acid*(S5)*	270×10^{-6} K^{-1}	Volume expansion coefficient of Stearic acid*(S6)*
C(Heat capacity)	1202 J/kg·K	Benzoic acid*(S7)*	1831.9 J/kg·K	Palmitic acid*(S8)*
k_{ba}(Thermal conductivity)	0.151 W/m·K	Benzoic acid linear fitting*(S9)*	0.171 W/m·K	Myristic acid linear fitting*(S10)*
Refractive index at vibrational resonance	1.45+0.87 i (1690 cm-1)	Benzoic acid *(S11)*	1.43+0.24 i (1710 cm^{-1})	Oleic acid*(S12)*
H_{eff} effective Hamaker constant	4.3×10^{-20} J	Benzoic acid *(S13)*	6.7×10^{-21} J	Palmitic acid*(S14)*

S4. PiFM of MBA layer on different substrates

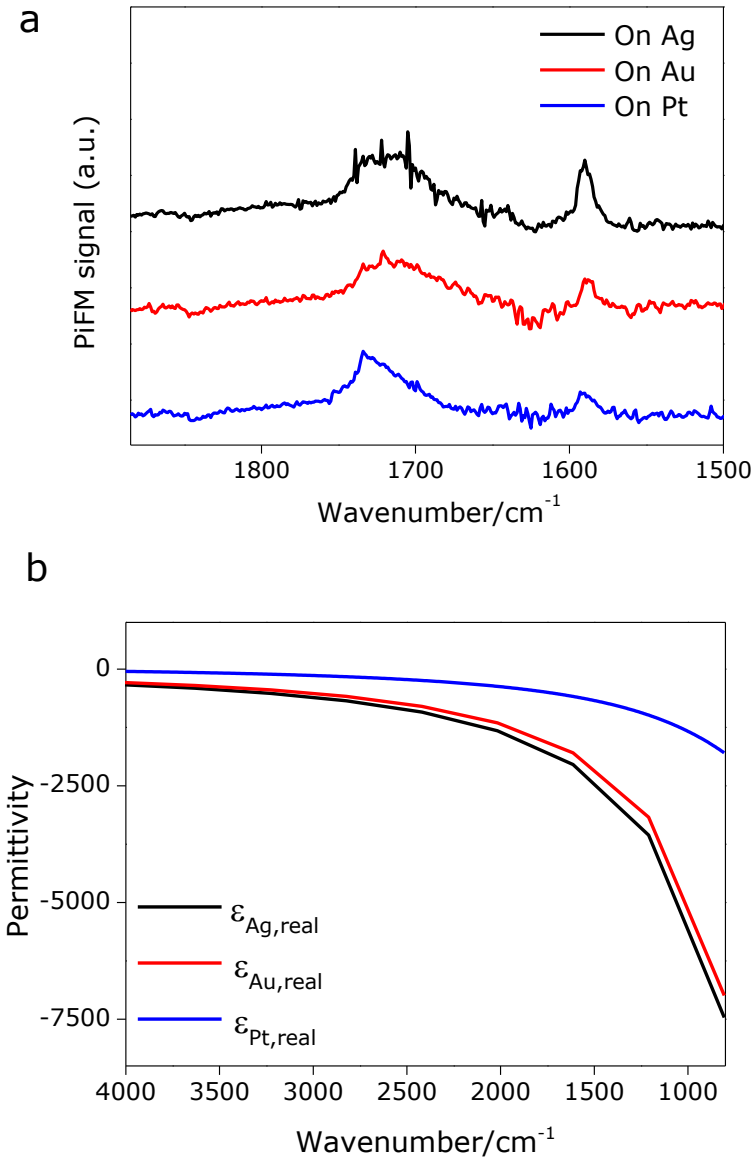

Figure S1. (a) PiFM spectra of MBA SAM on Ag, Au and Pt. (b) Permittivity real part plotting of Ag, Au and Pt in the recorded region. It is clear that the three metals are highly reflective in the mid-IR region. The refractive index data are from Ref *(S15-S16)*.

S5. AFM of Au film for imaging

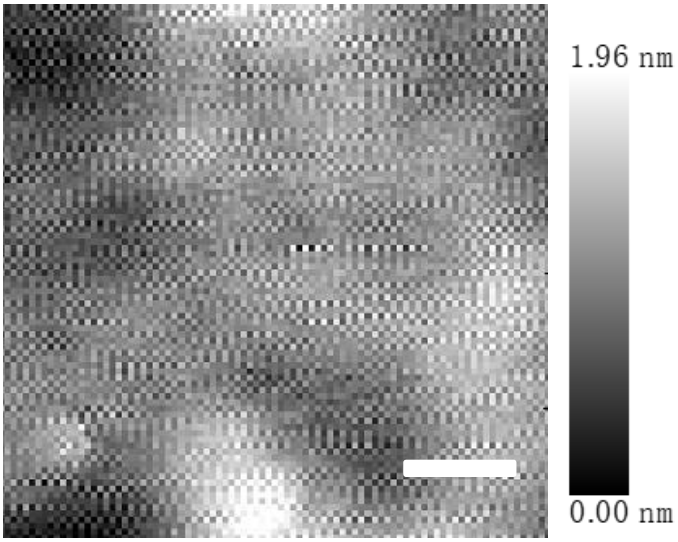

Figure S2. Topography of the gold. Scale bar: 100 nm.

S6. Hot spot simulation on Comsol

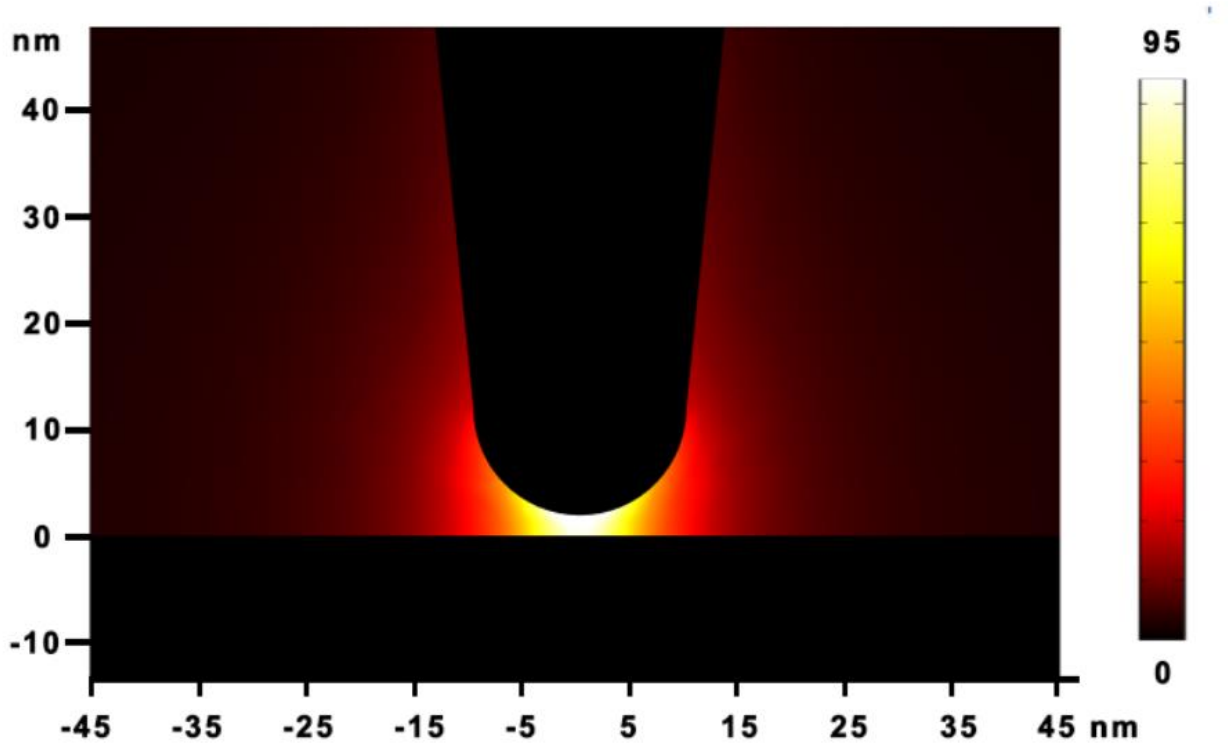

Figure S3. Field distribution of E field on the metal surface (xz plane). The hot spot was with around 5 nm diameter. Incident beam is set as p-polarized with 30 degree angle. The wavenumber is set as 1500 cm^{-1} as an arbitrary value while a whole IR region sweep does not show huge variation of the field distribution. The simulation is carried on comsol 3.5, scattering field is used to simulate the field distribution. The tip is set as a hemisphere with 10 nm radius head connected a cone with 30 nm end radius and 200 nm height. The substrate is set as SiO_2/Si with a 100 nm thickness gold film as the experiment condition.

S7. PiFM and FTIR of BSA

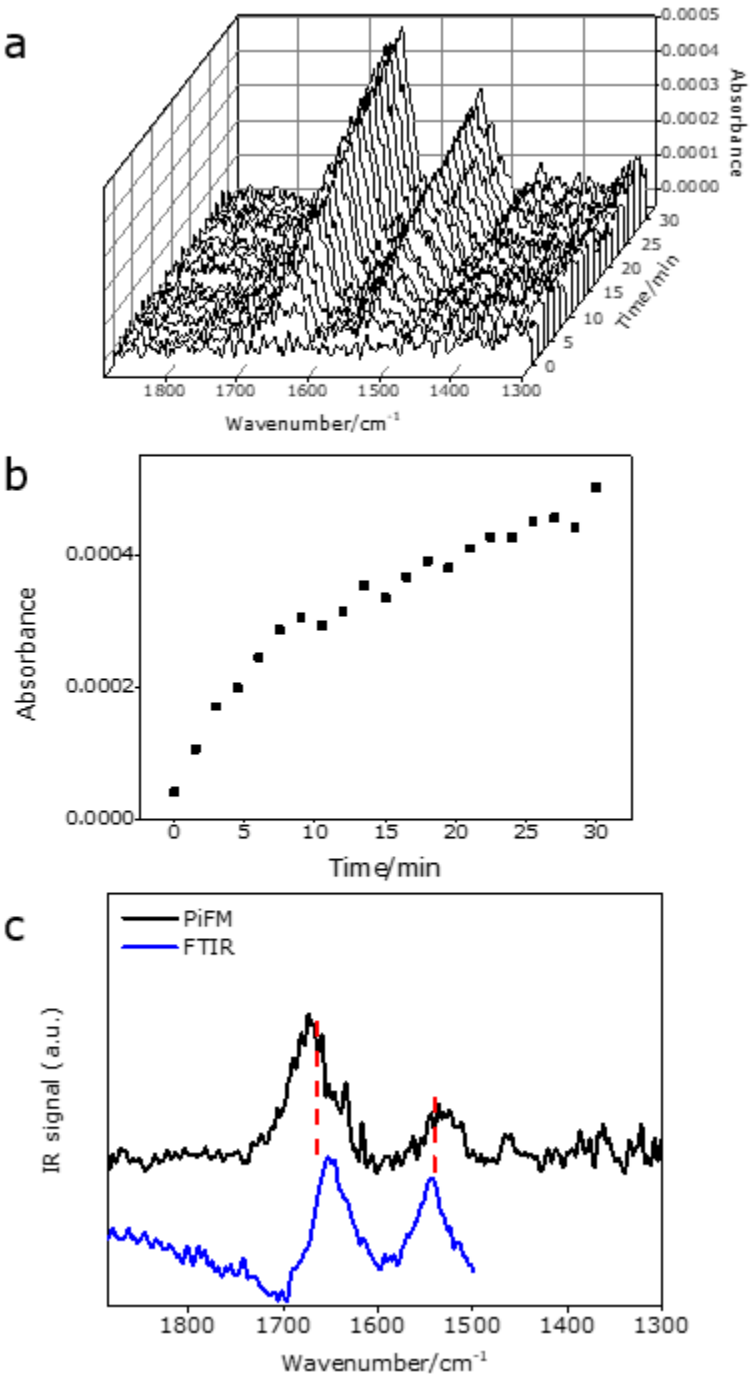

Figure S4. (a) Evolution of the antenna array enhanced ATR-SEIRAS spectra of 300 µL 100 ng/mL BSA solution (b) Plot of the absorption intensity of amid I (black squares) from BSA as a function of adsorption time (c) PiFM (black curve) and ATR-FTIR (blue curve) spectra of BSA on gold and in solution, respectively.

[S1] Bao, W. J.; Li, J.; Li, J.; Zhang, Q. W.; Liu, Y.; Shi, C. F.; Xia, X. H. Au/ZnSe-based surface enhanced infrared absorption spectroscopy as a universal platform for bioanalysis. *Anal. Chem.* **2018,** *90,* 3842-3848.
[S2] Hauer, B.; Engelhardt, A. P.; Taubner, T. Quasi-analytical model for scattering infrared near-field microscopy on layered systems. *Opt. Express* **2012,** *20,* 13173-13188.
[S3] Jahng, J.; Potma, E. O.; Lee, E. S. Tip-enhanced thermal expansion force for nanoscale chemical imaging and spectroscopy in photo-induced force microscopy. *Anal. Chem.* **2018,** *90,* 11054-11061.
[S4] Dazzi, A.; Glotin, F.; Carminati, R. Theory of infrared nanospectroscopy by photothermal induced resonance. *J. Appl. Phys.* **2010,** *107,* 124519.
[S5] Smith, E. R. The determination of the coefficient of cubical expansion of solid benzoic acid by means of a gas-filled dilatometer. *Bureau of Standards Journal of Research* **1931,** *382,* 903-905.
[S6] Engineering ToolBox, (2014). *Solids - Volume Temperature Expansion Coefficients.* [online] Retrieved from: https://www.engineeringtoolbox.com/volum-expansion-coefficients-solids-d_1894.html (19 th, November, 2018)
[S7] Furukawa, G. T.; McCoskey, R. E.; King, G. J. Calorimetric properties of benzoic acid from 0^{o} to 410^{o} K. *Journal of Research of the National Bureau of Standards,***1951,** *47,* 2251.
[S8] Saeed, R. M. Thermal characterization of phase change materials for thermal energy storage. Masters Theses, Missouri University, **2016**.
[S9] Sun, T.; Teja, A. S. Density, viscosity, and thermal conductivity of aqueous benzoic acid mixtures between 375 K and 465 K. *J. Chem. Eng. Data.* **2004,** *49,* 1843-1846.
[S10] Wang, X.; Sun, T.; Teja, A. S. Density, viscosity, and thermal conductivity of eight carboxylic acids from (290.3 to 473.4) K. *J. Chem. Eng. Data.* **2016,** *61,* 2651-2658.
[S11] Yamamoto, K. Akio, M. Complex refractive index determination of bulk materials from infrared reflection spectra. *Appl. Spectrosc.* **1995,** *49,* 639-644.
[S12] McGinty, S.; Kapala, M. K.; Niedziela, R. F. Mid-infrared complex refractive indices for oleic acid and optical properties of model oleic acid/water aerosols. *Phys. Chem. Chem. Phys.* **2009,** *11,* 7998-8004.
[S13] Croucher, M. D.; Halr, M. L. Hamaker constants and the principle of corresponding states. *J. Phys. Chem.* **1977,** *81,* 17.
[S14] Eom, N.; Parsons, D. F.; Craig, V. S. Measurement of long range attractive forces between hydrophobic surfaces produced by vapor phase adsorption of palmitic acid. *Soft. Matter.* **2017,** *13,* 8910-8921.
[S15] Babar, S.; Weaver, J. S. Optical constants of Cu, Ag, and Au revisited. *Appl. Opt.* **2015,** *54,* 477-481.
[S16] Rakić, A. D.; Djurišić, A. B.; Elazar, J. M.; Majewski, M. L. Optical properties of metallic films for vertical-cavity optoelectronic devices. *Appl. Opt.* **1998,** *37,* 5271-5283.